NAL TR-1267T

ISSN 0389-4010
UDC 532.517.4

TECHNICAL REPORT OF NATIONAL AEROSPACE LABORATORY

TR-1267T

A Computer Model for the Simulation of Turbulent Reacting Flow in a Jet Assisted Ram Combustor

Sanjiv KUMAR

1995年5月

NATIONAL AEROSPACE LABORATORY

CHŌFU, TOKYO, JAPAN

A Computer Model for the Simulation of Turbulent Reacting Flow in a Jet Assisted Ram Combustor*

Sanjiv KUMAR*1

ABSTRACT

A computer code for the simulation of the turbulent reacting flow in a jet assisted ram combustor is developed. Favre averaged Continuity and Navier-Stokes equations, equations for a low Reynolds number k-ε model and equations for mixture fraction and its variance are solved to simulate the turbulent reacting flow. A Stretched Laminar Flamelet Model (SLFM) in the mixture fraction space is used to simulate the combustion of Hydrogen and Air using a 28-step reaction mechanism with 10 species. The SLFM is coupled to the turbulent flow through density which is calculated using an assumed Beta-shaped probability distribution function for mixture fraction and a Log-normal probability distribution function for the scalar dissipation. All other mass averaged thermo-chemical variables are computed off-line after a converged solution has been achieved. Solution of the continuity equation and the three momentum equations is achieved using the SIMPLER algorithm. The linearised system of equations for each variable is solved sequentially using a Incomplete Lower Upper pre-conditioned conjugate gradient method. Simulation results showing the recirculation zones, distribution of species and temperature are presented.

Keywords: Turbulent Flow, Turbulent Combustion, Ram Combustor, Jet Stabilised Flame, Computer Model, Strained Laminar Flamelet Model.

概　　要

噴流保炎型ラム燃焼器の中の乱流火炎を，10個の化学種，28ステップの反応式を用いた伸長層流火炎片モデルで模擬した。連続，運動量，混合分率およびその変動などの3次元支配方程式に質量加重平均を適用した。乱れは低レイノルズ数$k-\varepsilon$モデルにより模擬し，やはり質量加重平均を用いた。熱化学量を計算するために推定確率密度関数（PDF）法を用いた。詳細には混合分率のPDFとしてβ－分布を用い，スカラー量消散のPDFとして対数正規分布を用いた。その他の熱化学量は解が収束したのち計算した。連続の式と運動量方程式の解はSIMPLERアルゴリズムを用いて求めた。不完全LU分解前処理付き共役勾配（ILU CG）法を線形化された式を解くために用いた。これらの結果得られた再循環領域，化学種および温度の分布を示した。

1. INTRODUCTION

Jet Assisted Ram Combustor is a novel concept and it relies on the turning jet to provide the flame holding which is ordinarily provided by a V-gutter in a conventional ram combustor. The jet can provide efficient mixing of the fuel and the oxidant as well as good flame stabilisation[1]. However experiments to study and develop an optimum design configuration for such combustors are extremely expensive and time consuming as numerous experiments are needed to investigate the various configurations. It is expected that a numerical model can help in designing specific experiments and to studv

* 平成7年2月14日　受付 (received 14 February 1995)
*1 原動機部 (Aeroengine Division)
STAフェロー (STA Fellow Ship)

various configurations numerically. With this objective, development of the numerical codes to simulate the turbulent combustion was started.

The modeling of turbulent combustion is an active area of research and poses numerous challenges to the engineer. This is because the physical and chemical processes taking place in a combustor are extremely complex interactions of the turbulent flow field and the finite rate chemistry. A complete rigourous description of these phenomena is still not possible and this necessitates the engineering compromises which must be made to realistically simulate such performance characteristics as efficiency, power output and pollutant formation. Furthermore such simulations provide an insight into improving the combustor performance and can be used to design better experiments economically which in absence of such simulations will have to rely on hit and trial methods alone. In the past several models of varying degree of complexity has been used to simulate the physical and chemical processes taking place in the combustors[2]. In general these models attempt to describe the turbulence, chemical kinetics and their mutual interaction using some simplifying assumptions.

An earlier report[3] presents the details of the computer model developed for the isothermal flow simulation. In the turbulent reacting flow case the governing equations are Favre averaged to eliminate the numerous density correlations that arise in the conventional averaged form.

Next the Favre averaged governing equations used to simulate the turbulent reactive flow are described.

2. GOVERNING EQUATIONS

The continuity and momentum equations are written as follows:

$$\frac{\partial(\bar{\rho}\tilde{u}_i)}{\partial x_i}=0 \tag{1}$$

$$\frac{\partial(\bar{\rho}\tilde{u}_j)}{\partial x_j}=-\frac{\partial \bar{P}}{\partial x_i}+\frac{\partial \bar{\tau}_{ij}}{\partial x_j}-\frac{\partial}{\partial x_j}(\bar{\rho}\widetilde{u_i''u_j''}) \tag{2}$$

where the mean shear stress $\bar{\tau}_{ij}$ is defined as follows:

$$\bar{\tau}_{ij}=\mu_l\left(\frac{\partial \tilde{u}_i}{\partial x_j}+\frac{\partial \tilde{u}_i}{\partial x_j}\right)-\frac{2}{3}\delta_{ij}\mu_l\frac{\partial \widetilde{u_m}}{\partial x_m} \tag{3}$$

Modified Boussinesq hypothesis is used to model the turbulent shear stress as follows:

$$\bar{\rho}\widetilde{u_i''u_j''}=-\mu_t\left(\frac{\partial \tilde{u}_i}{\partial x_j}+\frac{\partial \tilde{u}_j}{\partial x_i}\right)+\frac{2}{3}\delta_{ij}\left(\mu_t\frac{\partial \widetilde{u_m}}{\partial x_m}+\bar{\rho}\tilde{k}\right) \tag{4}$$

The tilde indicates Favre averaging and the bar denotes conventional averaging.

A low Reynolds number k-ε model is used to compute the turbulent viscosity as follows:

$$\mu_t=C_\mu f_\mu \bar{\rho}\frac{\tilde{k}^2}{\tilde{\varepsilon}} \tag{5}$$

The k-ε model has been used successfully in isothermal flow situation[3-5]. Since density weighted reacting flow can be considered similar to isothermal flow case, the same k-ε model is Favre averaged and is used to close the governing equations. Favre averaged k-ε models are most widely used methods for studying variable density turbulent flows[6]. Although such models have been used, it needs to be emphasized that the assumptions of the k-ε models remain nearly untested in variable density flows. Furthermore researchers have found ample evidence of counter-gradient flux in turbulent reacting flows which casts doubt on the validity of turbulent models based on gradient transport assumption[7-9]. However these models can still provide "reasonable" simulations at much lower computing costs than full Reynolds stress models and so tend to be a preferred choice for the engineer. Following are the modeled equations for the turbulent kinetic energy k and its dissipation ε:

$$\frac{\partial(\bar{\rho}\tilde{u}_j\tilde{k})}{\partial x_j}=\frac{\partial}{\partial x_j}\left[\left(\frac{\mu_t}{\sigma_k}+\mu_l\right)\frac{\partial \tilde{k}}{\partial x_j}\right]-\bar{\rho}\widetilde{u_i''u_j''}\frac{\partial \tilde{u}_i}{\partial x_j}-\frac{\mu_t}{\bar{\rho}^2}\frac{\partial \bar{\rho}}{\partial x_j}\frac{\partial \bar{P}}{\partial x_j}-\bar{\rho}\tilde{\varepsilon} \tag{6}$$

$$\frac{\partial(\bar{\rho}\tilde{u}_j\tilde{\varepsilon})}{\partial x_j}=\frac{\partial}{\partial x_j}\left[\left(\frac{\mu_t}{\sigma_\varepsilon}+\mu_1\right)\frac{\partial \tilde{\varepsilon}}{\partial x_j}\right]-C_{\varepsilon 1}f_1\frac{\tilde{\varepsilon}}{\tilde{k}}\left[\bar{\rho}\widetilde{u_i''u_j''}\frac{\partial \tilde{u}_i}{\partial x_j}+\frac{\mu_t}{\bar{\rho}^2}\frac{\partial \bar{\rho}}{\partial x_j}\frac{\partial \bar{P}}{\partial x_j}\right]-C_{\varepsilon 2}f_2\frac{\bar{\rho}\tilde{\varepsilon}^2}{\tilde{k}} \tag{7}$$

Further discussion on choice of this model is provided by Kumar[3]. The mixture fraction $\tilde{f}$ and its variance $\tilde{g}=\widetilde{f''^2}$ are calculated using the following

equations:

$$\frac{\partial(\bar{\rho}\tilde{u}_j\tilde{f})}{\partial x_j} = \frac{\partial}{\partial x_j}\left[\left(\frac{\mu_t}{\sigma_f} + \mu_l\right)\frac{\partial \tilde{f}}{\partial x_j}\right] \tag{8}$$

$$\frac{\partial(\bar{\rho}\tilde{u}_j\tilde{g})}{\partial x_j} = \frac{\partial}{\partial x_j}\left[\left(\frac{\mu_t}{\sigma_g} + \mu_l\right)\frac{\partial \tilde{g}}{\partial x_j}\right] + \frac{2\mu_t}{\sigma_f}\left[\left(\frac{\partial \tilde{f}}{\partial x_j}\right)\right]^2 - C_D\bar{\rho}\frac{\tilde{\varepsilon}\tilde{g}}{\tilde{k}} \tag{9}$$

3. TURBULENT NON-PREMIXED COMBUSTION MODEL

Combustion theory does not yet offer an universal approach to turbulent combustion modeling partly due to the range of turbulence chemistry interactions and partly due to lack of comprehensive understanding of fine scale turbulence. Consequently a range of turbulent combustion models with varying degree of complexity have been used by engineers. In general the combustion models can be classified into following four categories:

(1). Flame sheet model
(2). Equilibrium model
(3). Partial equilibrium model
(4). Non-equilibrium model

Flame sheet models are based on one step irreversible reaction and assume very fast chemistry and complete combustion. Modifications to account for intermediate products are possible. Obviously such models are too simplistic to account for the complex process taking place in the turbulent reactive flow.

The next category of model has been used widely in the past and it assumes fast chemistry and full chemical equilibrium to calculate the products of combustion. Equilibrium models can either be applied to one step irreversible reaction or through the use of combined variables to multi-step reactions. The number of species incorporated in the model depends on the detail chemistry desired. However such a model is an idealisation which cannot be applied to typical combusting flows due to wide range of relevant chemical and mixing time scales[7].

Partial equilibrium models introduce more realism by recognising that slower reactions are in partial equilibrium while faster reactions are in complete equilibrium. These models require a reaction progress variable in addition to the conserved scalar. The conserved scalar is usually chosen to be the mixture fraction, although it can be any judiciously combined species fraction. Such models have been used in the past to produce reasonable simulations of the turbulent combustion[10]

Non-equilibrium models attempt to incorporate realistic, detailed and finite chemistry to simulate the turbulent combustion. These models are capable of predicting extinction, re-ignition and super-equilibrium peaks of radicals. One way of modeling will be to include the complete detailed chemical mechanism and solve for all the species along with the Navier-Stokes and other governing equations. However this is a formidable task since the equations satisfied by the species mass fractions and the temperature are coupled with the other equations. Hence a strong incentive exists to decouple the chemistry problem from the turbulence problem. This has led to two approaches namely the Stretched Laminar Flamelet Model (SLFM) and the Conditional Moment Closure Model (CMCM).

In the case of SLFM, the turbulent non-premixed flame is viewed as consisting of thin reacting laminae, convected and stretched by turbulence[11]. Furthermore if their thickness is smaller than the Kolmogorov length scale, then they conserve the inner structure of a laminar flamelet. These flamelet structures are defined by the local chemical kinetics and the transport properties of the reacting species, and such an approach introduces these effects into the description of the turbulent flames[12].

On the other hand, the newly proposed Conditional Moment Closure Model,[13] does not rely on any local instantaneous structure of the reaction zone, but rather predicts averages conditioned on the local, instantaneous, value of the mixture fraction. Such models, however, increase the dimensionality of the problem and still need modeling assumptions to arrive at the evolution equations for conditional mean and variance. Some Direct Numerical Solutions confirm validity of both SLFM and CMCM, with CMCM shown to produce superior results if the average scalar dissipation rate conditioned on the mixture fraction is modeled prope-

rly[14,15].

In the present research SLFM is used to model the turbulent non-premixed combustion of H_2 and Air and the details of flamelet calculations are presented next.

4. STRETCHED LAMINAR FLAMELET MODEL

In principle a library of flamelets can be constructed using experimental data and such an approach was used by Liew[16]. However, in such an approach the flamelets must be converted from physical space to the conserved scalar space before they can be used in numerical modeling. Furthermore it is very difficult to achieve high levels of strain experimentally which is necessary if the finite chemistry is to be included in the model. For this reason many simulations include only one flamelet at some typical non-zero strain[16,17]. In this research, following Lentini[18] a library of flamelets is constructed in the conserved scalar space for 6 different strains. An inert case is included to simulate the case of infinite strain.

4. 1 Reaction Mechanism

A 25 step reaction mechanism for H_2 and air combustion and a 3 step Zeldovich mechanism for NOx production, involving a total of 10 species is used to calculate the laminar flamelets. The 10 species used in the modeling are H_2, O_2, N_2, H_2O, H, O, N, OH, HO_2 and NOx. The reaction mechanism used is same as described by Dixon-Lewis and Missaghi[19] and is given in Table I for completeness. Included are the Zeldovich mechanism (last three reactions in Table I) and forward rate coefficients k_f. The forward rate coefficients are expressed as $k_f = AT^B \exp(-C/T)$ unless otherwise stated and are expressed in appropriate cm, mol, s units.

Table I Reaction Mechanism

	reaction	A	B	C
1	$OH+H_2=H_2O+H$	1.1×10^{9}	1.3	1825
2	$H+O_2=OH+O$	4.2×10^{15}	−0.46	8450
3	$O+H_2=OH+H$	1.8×10^{5}	2.5	3300
4	$H+O_2+H_2=HO_2+H_2$	2.8×10^{18}	−0.86	0
5	$H+O_2+N_2=HO_2+N_2$	3.75×10^{20}	−1.72	0
6	$H+O_2+O_2=HO_2+O_2$	3.0×10^{20}	−1.72	0
7	$H+O_2+H_2O=HO_2+H_2O$	9.4×10^{18}	−0.76	0
8	$H+HO_2=OH+OH$	2.2×10^{14}	0	710
9	$H+HO_2=O+H_2O$	5.0×10^{12}	0	710
10	$H+HO_2=H_2+O_2$	2.16×10^{13}	0	280
11	$OH+HO_2=H_2O+O_2$	1.8×10^{13}	0	0
12	$O+HO_2=OH+O_2$	2.0×10^{13}	0	0
13	$H+H+H_2=H_2+H_2$	9.2×10^{16}	−0.6	0
14	$H+H+N_2=H_2+N_2$	1.0×10^{18}	−1.0	0
15	$H+H+O_2=H_2+N_2$	1.0×10^{18}	−1.0	0
16	$H+H+H_2O=H_2+H_2O$	6.0×10^{19}	−1.25	0
17	$H+OH+H_2=H_2O+H_2$	1.6×10^{22}	−2.0	0
18	$H+OH+O_2=H_2O+O_2$	1.6×10^{22}	−2.0	0
19	$H+OH+N_2=H_2O+N_2$	1.6×10^{22}	−2.0	0
20	$H+OH+H_2O=H_2O+H_2O$	8.0×10^{22}	−2.0	0
21	$H+O+H_2=OH+H_2$	6.2×10^{16}	−0.6	0
22	$H+O+O_2=OH+H$	6.2×10^{16}	−0.6	0
23	$H+O+N_2=OH+N_2$	6.2×10^{16}	−0.6	0
24	$H+O+H_2O=OH+H_2O$	3.1×10^{17}	−0.6	0
25	$OH+OH=O+H_2O$	$k_f=\exp(27.1+1.5\times10^{-3}T)$		
26	$O_2+N=NO+O$	6.4×10^{9}	1.0	3149
27	$N_2+O=NO+N$	1.8×10^{14}	0	38342
28	$N+OH=NO+H$	3.0×10^{13}	0	0

4. 2 Flamelet Calculation Details

Flamelets are calculated in the conserved scalar space of mixture fraction. The mixture fraction f is defined as follows:

$$f=\frac{Z_j-Z_{j,o}}{Z_{j,f}-Z_{j,o}} \qquad j=1,\ 2,\ \cdots\cdots,\ L \tag{10}$$

where Z_j is the elemental mass fraction of the L elements involved in the N species reacting mixture. Subscripts f and o denote fuel and oxidant respectively. The evolution of f is given by Equation 8. This assumes that all species have the same diffusion coefficients. Furthermore if Dufour terms and Soret effects are assumed negligible, and an assumption of equal diffusivities of species and heat is introduced, then the governing equation for energy assumes the same form as that of the Equation 8. This means that solution of Equation 8 provides a solution of the energy equation under the above simplifying assumption and in this case the definition of mixture fraction f is as follows:

$$f=\frac{h-h_o}{h_f-h_o} \tag{11}$$

where h is the enthalpy of the reacting mixture. It should be noted, however, that the energy equations will need extra terms if either the kinetic energy per unit mass of mixture is not small compared to the mixture enthalpy per unit mass as in the case of supersonic flows or if radiation effects are to be included.

The state variables to be determined across the flamelet profile are the species mass fractions Y_i ($i=1,2,\ldots,\ N$) and the temperature T, assuming pressure to be thermo-chemically constant[18] Now the governing equation in the conserved scalar space is given as follows[11] :

$$\frac{\partial Y_i}{\partial t}-\frac{\zeta}{2}\frac{\partial^2 Y_i}{\partial f^2}=\dot{\tau}_i \qquad (i=1,\ 2,\ \cdots\cdots,\ N) \tag{12}$$

where τ_i is the net production rate per unit mixture mass of species i. The scalar dissipation rate ζ is defined as follows:

$$\zeta=2D\frac{\partial \mathrm{f}}{\partial x_i}\frac{\partial \mathrm{f}}{\partial x_i} \tag{13}$$

where D is the molecular diffusivity of f.

Several laminar flow configurations can be used to incorporate the flow dependent effects in a flamelet. For the case of diffusion flamelets the configuration of counter-flow geometry seems to be an appropriate choice[20] based on the assumption that flamelets of the mixing layer types are predominant in turbulent diffusion flame. The steady one-dimensional equations for the counter-flow geometry then can be solved in terms of a similarity coordinate and the instantaneous scalar dissipation rate ζ can be calculated as follows:

$$\zeta=\frac{a}{\pi}e^{-2\,[erfc^{-1}(2f)]^2} \tag{14}$$

where a is the strain rate usually taken as the velocity gradient at the stagnation point and $erfc$ denotes the complementary error function and $erfc^{-1}$ is its inverse.

For the general reaction system involving N chemical species and R reaction steps of the form:

$$\sum_{i=1}^{N}\nu'_{ij}M_i=\sum_{i=1}^{N}\nu''_{ij}M_i \qquad j=1,\ 2,\ \cdots,\ R \tag{15}$$

where Mi is the chemical symbol for species i, ν'_{ij} and ν''_{ij} are the stoichiometric coefficients for species i appearing as reactant and product respectively, in reaction j, the net rate of change of concentration of this species i due to the reaction j is given by the Arrhenius expression as follows:

$$\dot{c}_{ij}=(\nu''_{ij}-\nu'_{ij})\left[k_{fj}\rho^{o_f}\prod_{m=1}^{N}\left(\frac{Y_m}{W_m}\right)^{\nu'_{ij}}-k_{bj}\rho^{o_b}\prod_{m=1}^{N}\left(\frac{Y_m}{W_m}\right)^{\nu''_{ij}}\right] \tag{16}$$

where W is the molecular weight and $o_f=\Sigma_i\nu'_{ij}$ and $o_b=\Sigma_i\nu''_{ij}$ are overall orders of forward and backward reactions j. k_f and k_b are the forward and backward reaction rates. The forward reaction rates for each reaction is specified in Table 1. The equilibrium constant for each reaction is evaluated by calculating the standard free energy change, which then is used to calculate the backward reaction rates. All the thermodynamic properties of the species are calculated using the least square coefficients given by Gordon and McBride[21]

Now the net production rate per unit mixture mass of species i can be defined as follows:

$$\dot{\tau}_i=\frac{W_i}{\rho}\sum_{j=1}^{R}\dot{c}_{ij} \tag{17}$$

The equation set 12 is solved using a time marching scheme over the range [0, 1] of the mixture fraction f and temperature is obtained by inverting the calorific equation of state:

$$h=\sum_{i=1}^{N} Y_i h_i\ (T) \tag{18}$$

The inversion of the above equation is performed using Newton's method. Once a steady state solution is obtained the procedure is repeated for different strain rate value to construct the library of flamelets.

The calculated library of flamelets is shown in Figures 1 to 7. Figure 1 shows the maximum temperatures obtained at different strains and resembles the top part of a typical S-shaped curve. These flamelets were calculated assuming H_2 to be at 300K, air to be at 600K and the pressure to be atmospheric. Under these conditions extinction occurs at a strain rate of $10000s^{-1}$ and the maximum temperature at extinction is 1603K. These values compare well with the computations of Dixon-Lewis and Missaghi[19] who obtained a peak temperature of 1422K at the extinction strain rate of $13000s^{-1}$. In their calculations the boundary conditions in the physical space are different but it can approximately correspond to both H_2 and air being at 300K. The profiles of temperature, H_2O, H, O, OH and NO are shown in Figures 2 to 7 respectively. The super-equilibrium peaks of the radicals H, O and OH are clearly observable in Figures 4, 5 and 6 respectively.

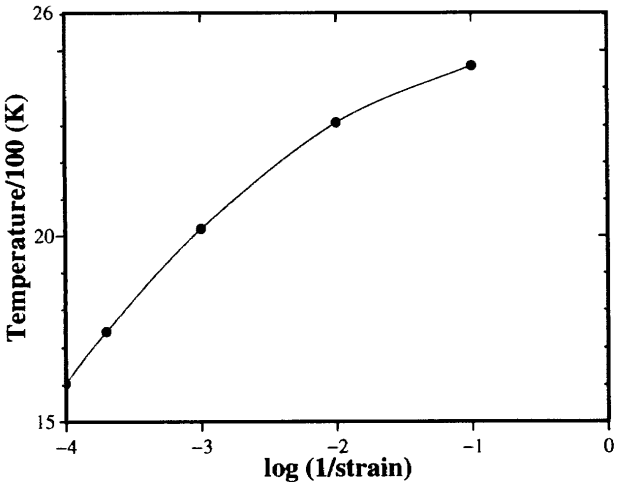

Fig. 1 Peak temperature in H_2-air diffusion flame as a function of the strain rate

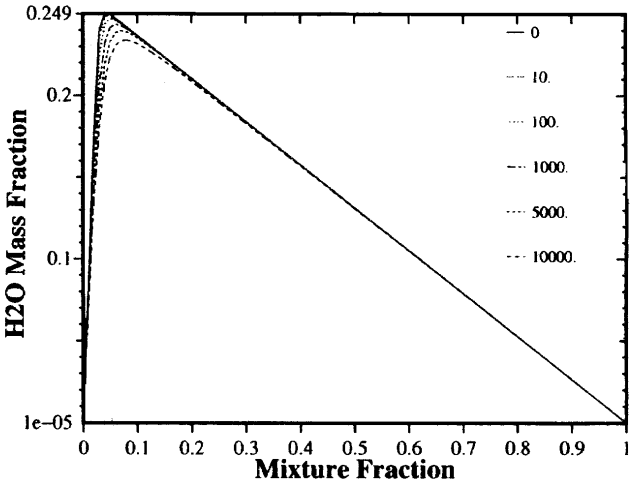

Fig. 3 Profiles of H_2O mass fraction as a function of strain rate

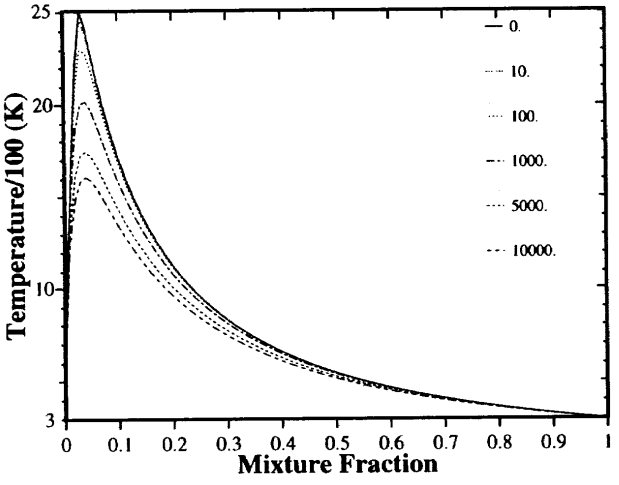

Fig. 2 Profiles of temperature in H_2-air diffusion flame as a function of strain rate

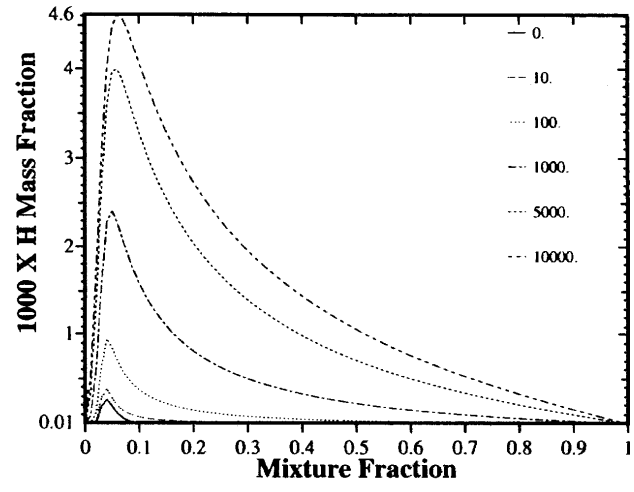

Fig. 4 Profiles of H mass fraction as a function of strain rate

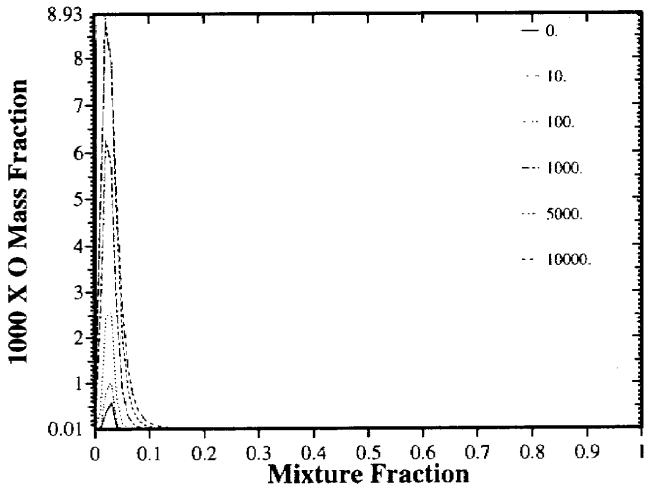

Fig. 5 Profiles of O mass fraction as a function of strain rate

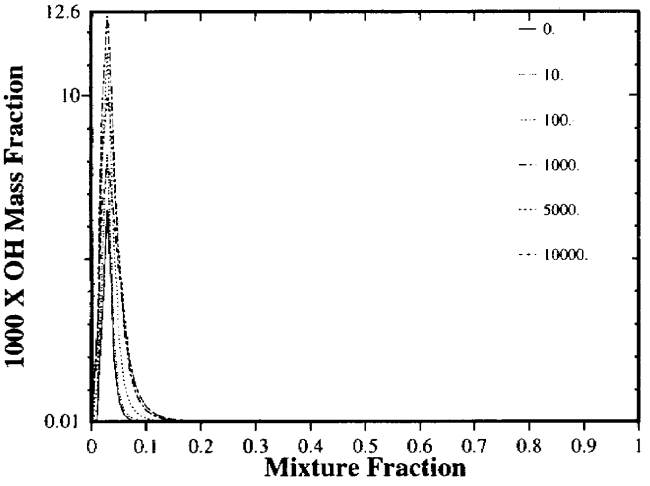

Fig. 6 Profiles of OH mass fraction as a function of strain rate

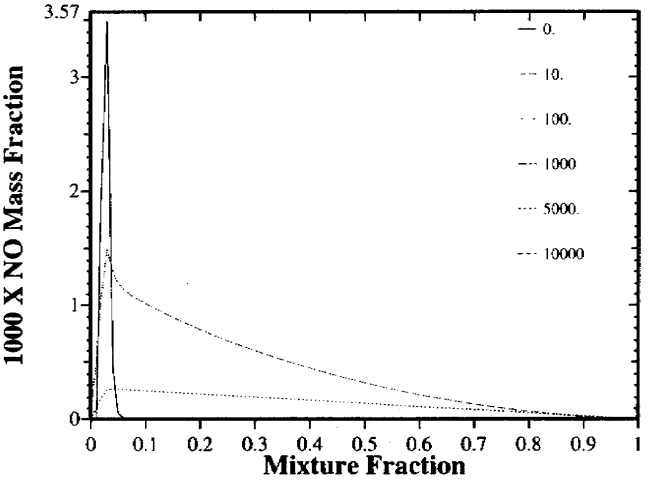

Fig. 7 Profiles of NO mass fraction as a function of strain rate

5. PDF CHEMISTRY CLOSURE

The next most important question relates to finding mean values for the thermo-chemical variables and reaction rates because turbulent flows lead to "unmixedness". Because of this "unmixedness" one cannot compute mean reaction rates on the basis of mean concentrations but it ought to be computed as mean of the reaction rates based on instantaneous concentrations. Further since mean density couples the chemistry with the flow, its accurate calculation is vital. A most common approach is to use Probability Density Function (PDF) which can be either derived[22] or assumed. In the latter case the method is known as the presumed-PDF method and is used in this research.

The flamelets in the strain space are characterised by ζ_{max} corresponding to the maximum temperature location[16]. Now if $\phi = \phi(f, \zeta_{max})$ is the instantaneous value of any state quantity inside the flamelet, the mean value can be determined by introducing the bivariate pdf $P(f, \zeta_{max})$ as

$$\overline{\phi} = \int_0^\infty \int_0^1 \phi(f, \zeta_{max}) P(f, \zeta_{max}) \, df d\zeta_{max} \quad (19)$$

It is now assumed that f and ζ_{max} are statistically independent[12,16,20] and thus

$$P(f, \zeta_{max}) = P(f) P(\zeta_{max}) \quad (20)$$

In the presumed-pdf method, the two probability density functions are prescribed. A common choice is to assume β-probability density function for $P(f)$ and log-normal distribution for $P(\zeta_{max})$. Thus the following are prescribed:

$$P(f) = \frac{f^{a-1}(1-f)^{b-1}}{\int_0^1 f^{a-1}(1-f)^{b-1} \, df} \quad (21)$$

where

$$a = \tilde{f}\left[\frac{\tilde{f}(1-\tilde{f})}{\widetilde{f''^2}} - 1\right] \quad (22)$$

$$b = (1-\tilde{f})\left[\frac{\tilde{f}(1-\tilde{f})}{\widetilde{f''^2}} - 1\right] \quad (23)$$

Arguments parallel to Kolmogorov's third hypothesis lead to the conclusion that scalar dissipation rate is log-normally distributed[23] Hence the pdf in

the ζ_{max} space is prescribed to be a log-normal distribution as follows:

$$P(\zeta_{max}) = \frac{1}{\zeta_{max}\sigma\sqrt{2\pi}} \exp\left\{-\frac{1}{2\sigma^2}(ln\,\zeta_{max}-\mu)^2\right\} \tag{24}$$

where $\zeta_{max}\exp(\mu+\frac{\sigma^2}{2})\cdot\sigma$ is prescribed and μ is calculated following Lentini[12]. The scalar dissipation rate is modeled as follow:

$$\widetilde{\zeta}_{max} = C_D \frac{\widetilde{f''^2}\,\tilde{\varepsilon}}{\tilde{k}} \tag{25}$$

In order to evaluate Favre averaged density, temperature and species concentration one needs to evaluate the double-integral given by Equation 19 which will add excessively to the computational burden. In order to circumvent this problem, an approach suggested by Lentini[12] is followed to evaluate the mean densities using a 18th order orthogonal polynomial fit to the density profiles across the flamelets. It should be noted that the average density is the only quantity needed at each computational step. The other averaged quantities like temperature and species concentrations are computed by direct numerical evaluation of the double integrals after a converged solution is obtained. For this purpose a cubic spline interpolation scheme is used to generate 1000 integration points in the f-space.

6. MODEL CONSTANTS

The various constants used for the models are summarised below:

$C_\mu = 0.09$

$C_{\varepsilon 1} = 1.4$

$C_{\varepsilon 2} = 1.8$

$\sigma_k = 1.4$

$\sigma_\varepsilon = 1.3$

$f_\mu = \left(1+\frac{3.45}{\sqrt{Re_t}}\right)\left(1-e^{(-\frac{y^+}{70})}\right)$

$f_2 = \left(1-\frac{2}{9}\,e^{-(\frac{Re_t}{6})^2}\right)\left(1-e^{(-\frac{y^+}{5})}\right)^2$

$\sigma_f = 0.7$

$\sigma_g = 0.7$

$C_D = 2.0$

$\sigma = 2.0$

The terms Re_t and y^+ are defined as follows:

$$Re_t = \frac{k^2}{\nu\varepsilon} \text{ and } y^+ = \frac{\sqrt{ky}}{\nu}$$

where y is the normal distance from the wall and ν is the kinematic viscosity.

7. GRID LAYOUT

The cylindrical combustor has 8 nozzles placed round the circumference. The diameter of the combustor is 0.155m and its length is 0.670m. Due to the geometrical symmetry only one nozzle was modeled. The variable spacing grid used for modeling has 187272 control volumes in the computa-

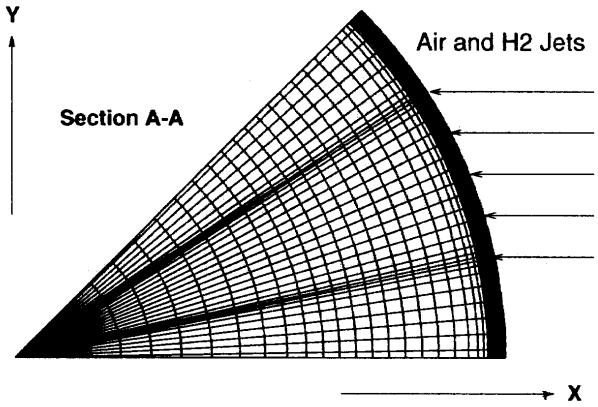

Fig. 9 Grid in X-Y plane

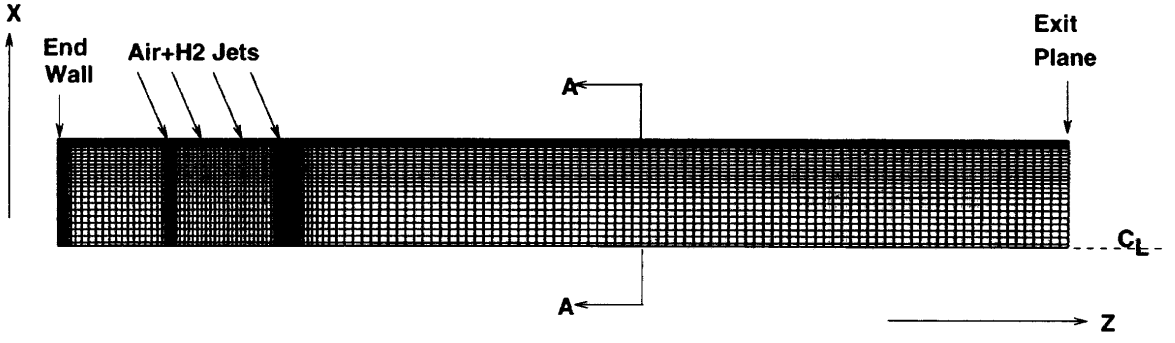

Fig. 8 Grid in X-Z plane

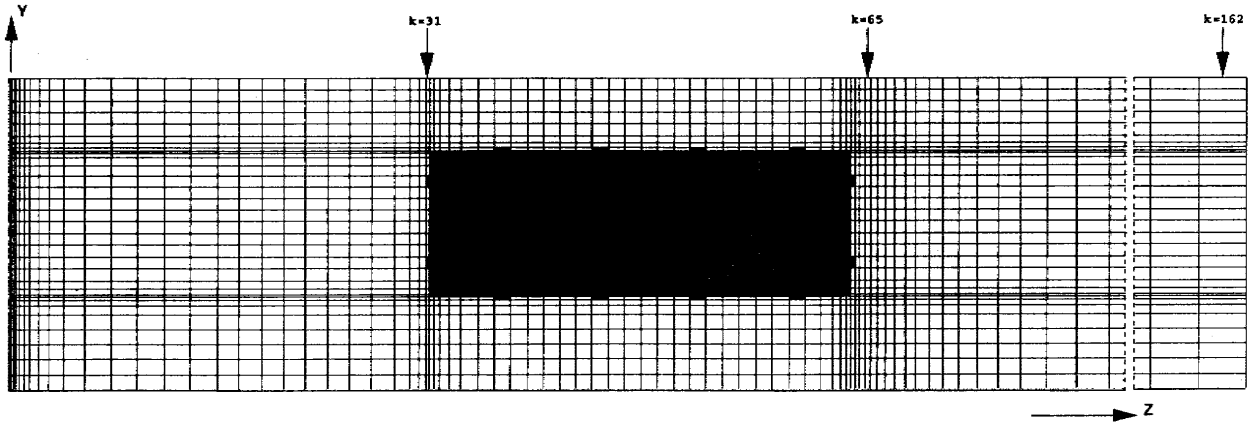

Fig. 10 Grid in Y-Z plane showing H_2 and air jet placements

tional region ($34 \times 34 \times 162$ in the x, y, and z directions) and is shown in Figure 8. The section A-A which lies in the x-y plane is shown in Figure 9.

Hydrogen is injected through 28 orifices of 1.5mm diameter placed around each nozzle. In these simulations the flow through 28 orifices is simulated by 12 control volumes having same flow area as the 28 orifices. The lay out of the H_2 and air nozzles is shown in Figure 10. The 12 protruding shaded rectangles are used for H_2 injection. Through the remainder of the shaded rectangular area air jet comes into the combustor. In future work the full resolution of the orifices will be attempted.

8. INITIAL AND BOUNDARY CONDITIONS

The air jet velocity at the inlet is 60m/s and is inclined at 30° towards the exit. The inlet air temperature is 600K. These conditions correspond to a Reynolds number in excess of 30000. H_2 injection was simulated by specifying the mixture fraction to be unity in the 12 control volumes placed uniformly around the air jet. The temperature of H_2 is assumed to be 300K. These simulations were carried out for the equivalence ratios of 0.2 and 1.0. At these conditions the injection velocity of the H_2 fuel was about 225m/s and 1012m/s respectively. For the walls and the center line zero-gradient boundary conditions are applied for all the variables. At the exit plane zero-gradient boundary conditions are specified for all the variables except pressure which is assumed to be atmospheric. For the boundaries in the angular directions, symmetry boundary conditions are applied.

9. COMPUTATIONAL DETAILS

All the governing equations are transformed to an arbitrary coordinate system (ξ, η, γ) and the resulting equations are discretized using the power law scheme of Patankar[24]. Furthermore such an approach has the advantage that the body fitted coordinate system can be easily used. Additional advantages include uniform mesh in the computational space, insensitivity of the convergence rate to the choice of under-relaxations factors. Further, the convergence rate is proportional to $\sqrt{N}$, where N is the number of grid points used and not to N as would be the case in Cartesian coordinates[3]. More details of the transformation can be found in Kumar[3].

The dependent variables are stored in a staggered fashion in order to avoid the chequer-board pattern that may result when all the variables are stored at the same grid location. A more detailed discussion of this can be found in Patankar[24]. Velocities are stored on the control volume faces while all scalars are stored at the control volume centers. Thus u, v and w velocities are stored on the ξ, η, and γ faces respectively.

SIMPLER algorithm is employed for the solution of continuity and momentum equations. Detailed derivation of the pressure correction equation and the pressure equations can be found in an earlier report[3]. The system of linearised equations for each variable is solved using a pre-conditioned conjugate gradient method. The pre-conditioner used is an incomplete lower upper factorisation of the coef-

ficient matrix.

The convergence rate of the SIMPLER algorithm for the simulation of turbulent reacting flow in the present problem is extremely poor and it was necessary to use small under-relaxation factors. Apart from varying density, it appears that the grid aspect ratios near the walls also contribute to the poor convergence behavior. Near the walls fine grids are necessary as these simulations do not rely on wall functions. Consequently, it was not possible to reduce errors to very low values in a reasonable computer time. These simulations were produced in about 100 hours of CPU time of a Cray Y-MP M92 machine with one processor. No appreciable change was observable by continuing the runs for longer time and so simulations were stopped after 100 hours even though the absolute sum of the errors in mass for all the 187272 control volumes was about 6% of the total mass flow. Although errors are higher than one would like it to be, these simulations provide a first and valuable insight into the flow and mixing patterns as well as the the combustion characteristics of the combustor.

10. RESULTS AND DISCUSSION

Simulation results for the equivalence ratios of 0.2 and 1.0 are presented. Two cross-sections are chosen for showing the computed contours of various quantities. These cross-sections are $K=31$ and $K=65$ and the location of these sections are indicated in Figure 10. In each figure two cases corresponding to the two equivalence ratios, at the same location, are shown. The left part of the figure corresponds to $\phi=0.2$ while the right part corresponds to $\phi=1.0$.

In Figure 11 the temperature contours are shown. Higher temperatures are obtained in the leaner case, however combustion is much more intense in the case of $\phi=1.0$ as can be seen in Figure 11(b). Also in both cases a very fractal type of structure emerges. These structures are like pieces of boomerangs stuck together in some fashion. In Figure 12 the contours of H_2O mass fraction (in percentage) are shown. The predicted maximum of H_2O mass fraction is same in both cases but as expected the region of H_2O formation is much wider in the case of $\phi=1.0$.

Formation of radicals such as H, O and OH are shown in Figures 13, 14 and 15 respectively. In all cases the super-equilibrium peaks of these radicals are observed. Furthermore the levels of these radicals for the two different equivalence ratios seems to be quite comparable. However NO formation seems to be much higher in the case of the lean mixture as can be seen in Figure 16. Also the regions of maximum NO formation do not always coincide with regions of maximum temperature. This is expected in real flames where super-equilibrium peaks of radicals like H, O and OH cause the NO formation to be different than one can observe from equilibrium chemistry considerations alone.

Figures 17 to 22 show the same contours at another section in the combustor. Again several boomerang type of structures are observable in the case of temperature as shown in Figure 17. Combustion does not seem to penetrate towards the center in the case of leaner mixture while it has nearly reached the center line in the case of unity equivalence ratio. H_2O contours are shown in Figure 18. The regions of H_2O formation seems to be considerably thicker than the regions of near maximum temperatures. The combustion activity seems to be quite intense in $K=65$ section in the case of $\phi=1.0$ while such is not the case for $\phi=0.2$. It appears that the momentum of the fuel jet is not enough in the case of $\phi=0.2$ to penetrate the potential core of air jet that develops downstream in such a configuration of the air nozzles.

Finally in Figure 23 streamlines colored by the density are shown in a section along the length of

Table II Overall Characteristics

ϕ	Pressure Loss Ratio	Mean Exit Temperature	NO_x Emission Index
	%	K	gm NO_x/kg Fuel
0.2	0.88	739	2.
1.0	2.02	1568	44.

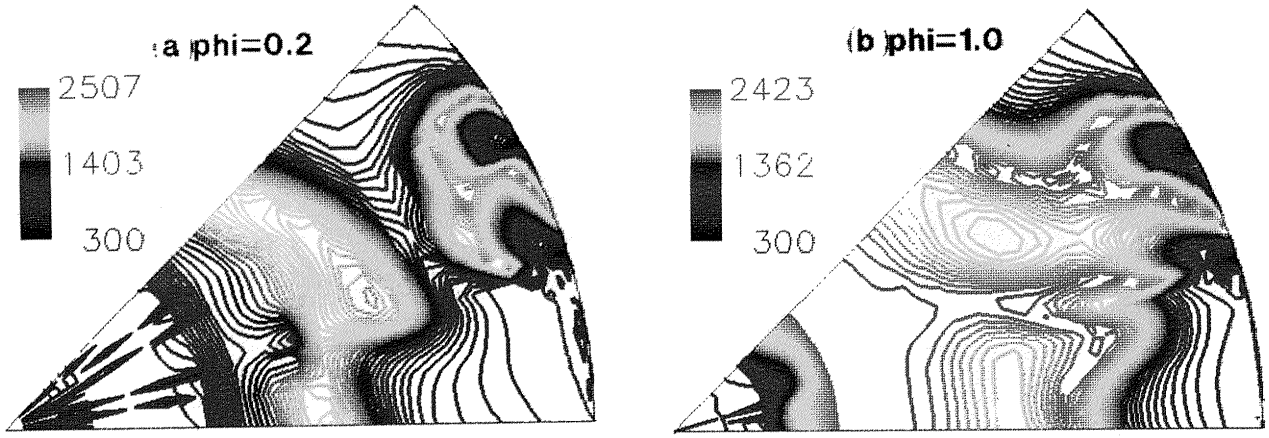

Fig. 11 Temperature contours (K=11)

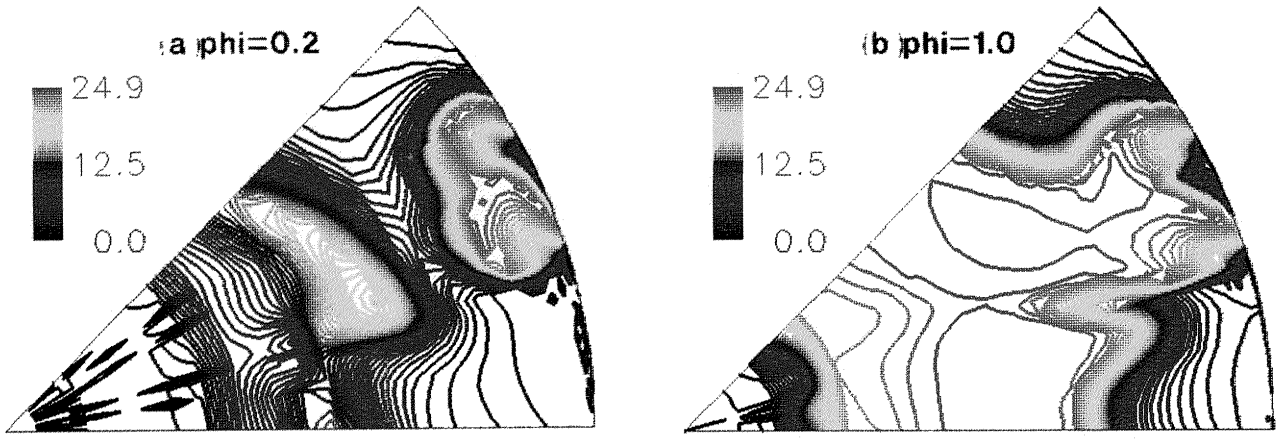

Fig. 12 Contours of H_2O mass fraction ($\times$=100)(K=31)

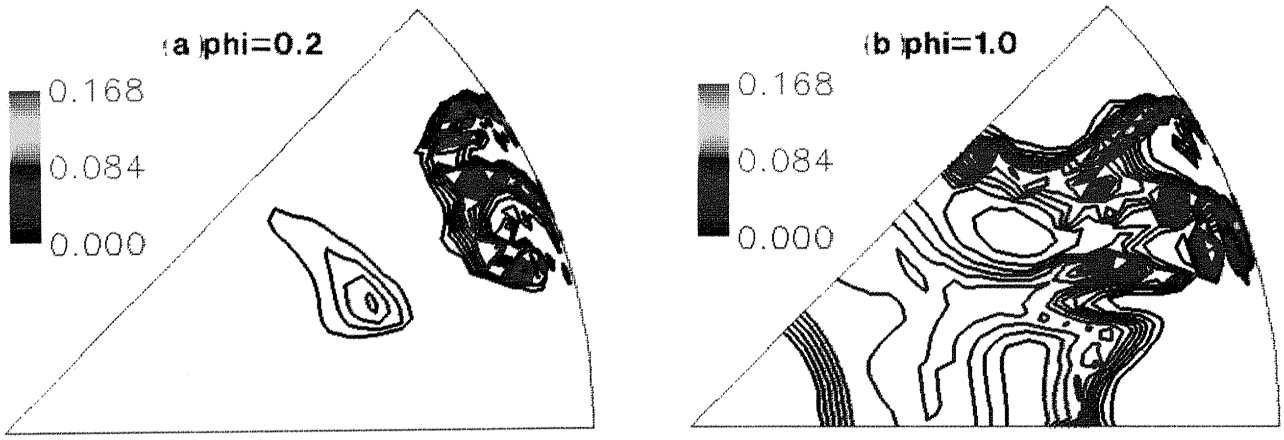

Fig. 13 Contours of H mass fraction ($\times$100)(K=31)

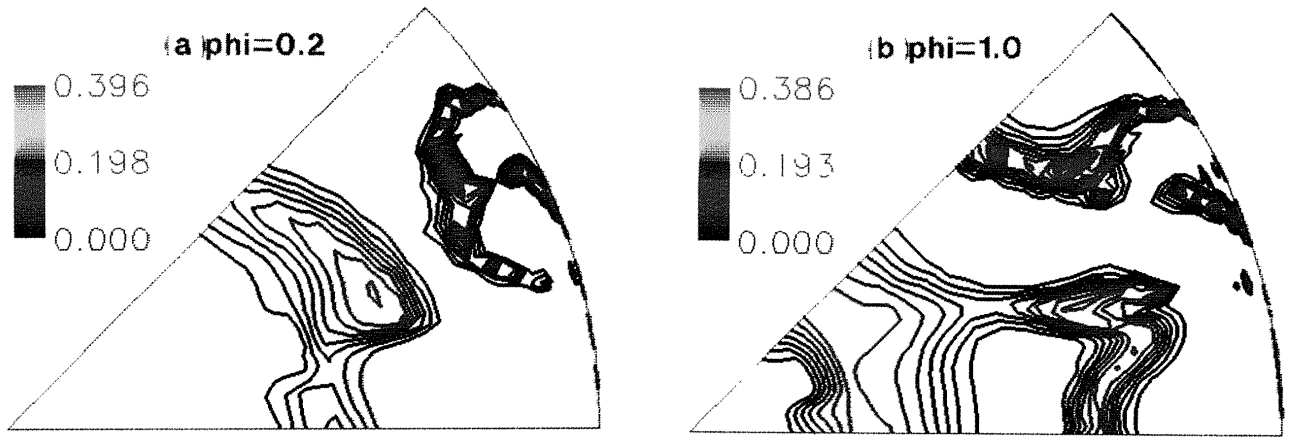

Fig. 14 Contours of O mass fraction($\times 100$)($K=31$)

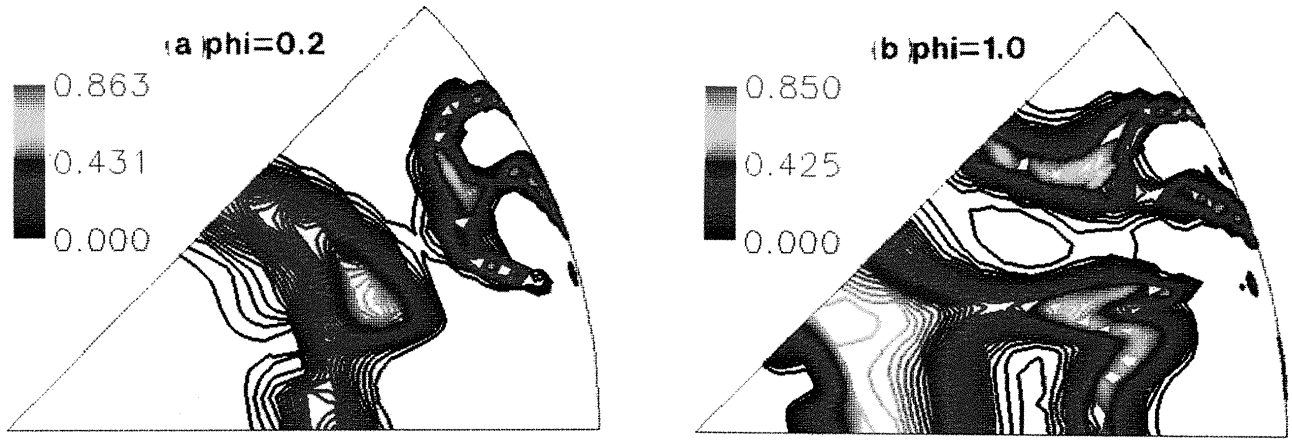

Fig. 15 Contours of OH mass fraction ($\times 100$)($K=31$)

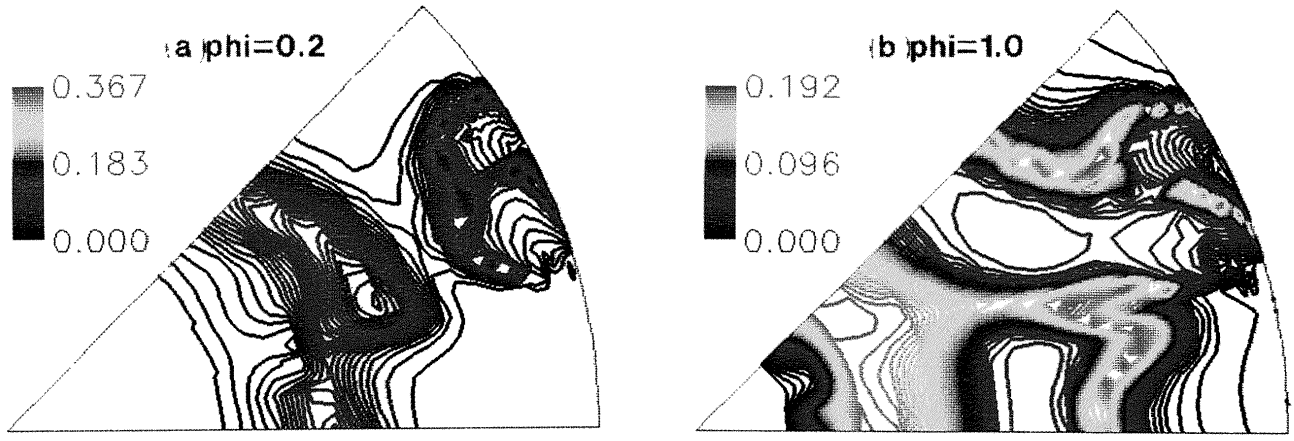

Fig. 16 Contours of NO mass fraction ($\times 100$)($K=31$)

Fig. 17 Temperature contours (K=65)

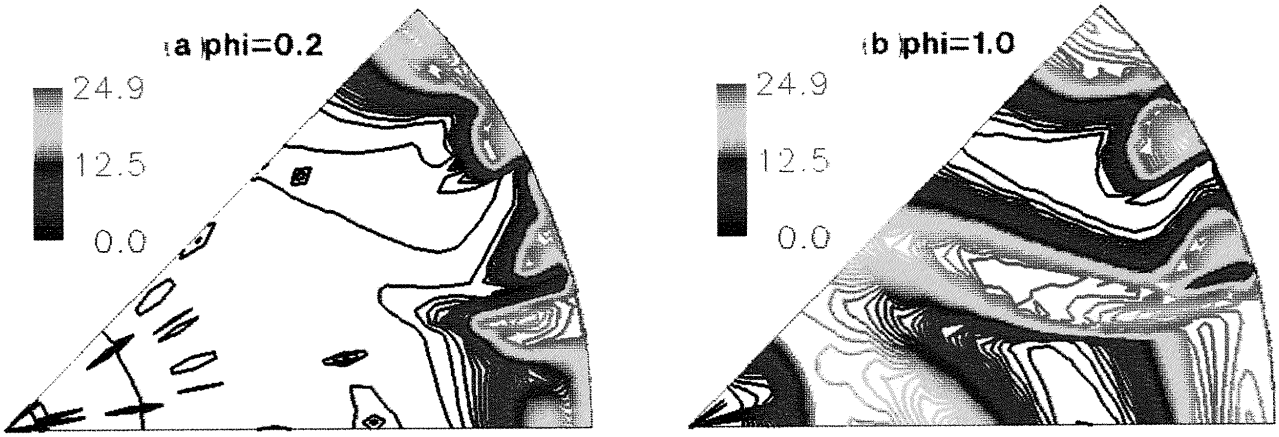

Fig. 18 Contours of H_2O mass fraction ($\times 100$)(K=65)

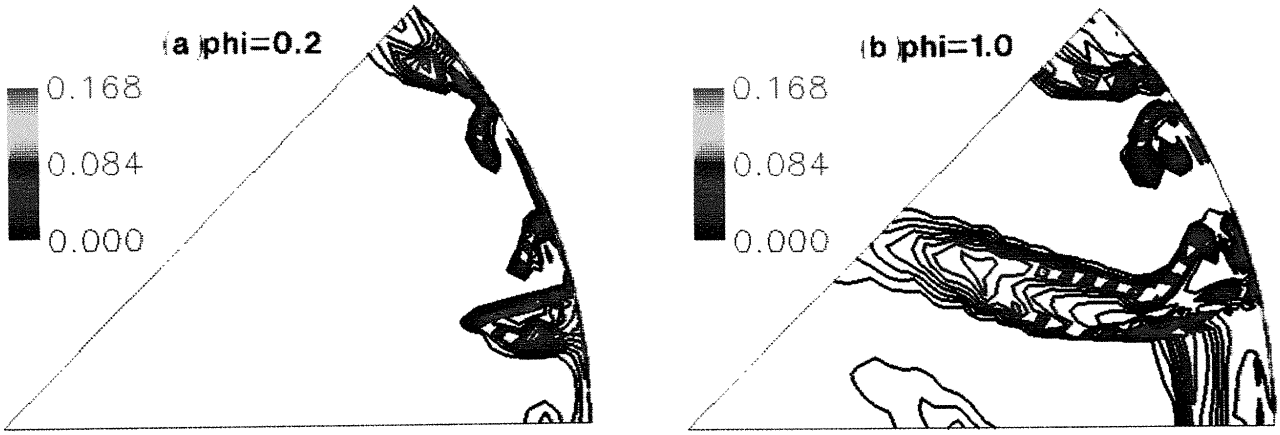

Fig. 19 Contours of H mass fraction($\times 100$)(K=65)

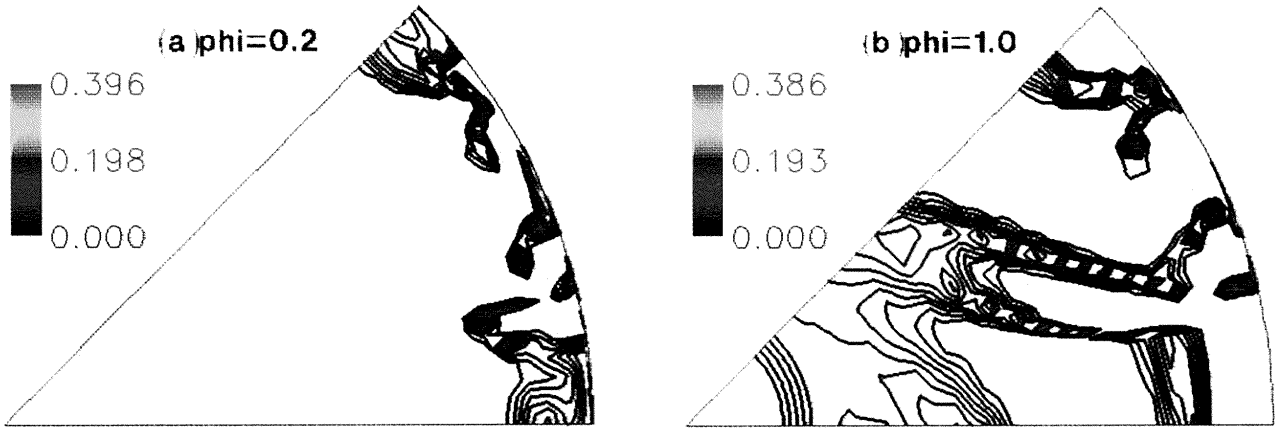

Fig. 20 Contours of O mass fraction($\times 100$)(K=65)

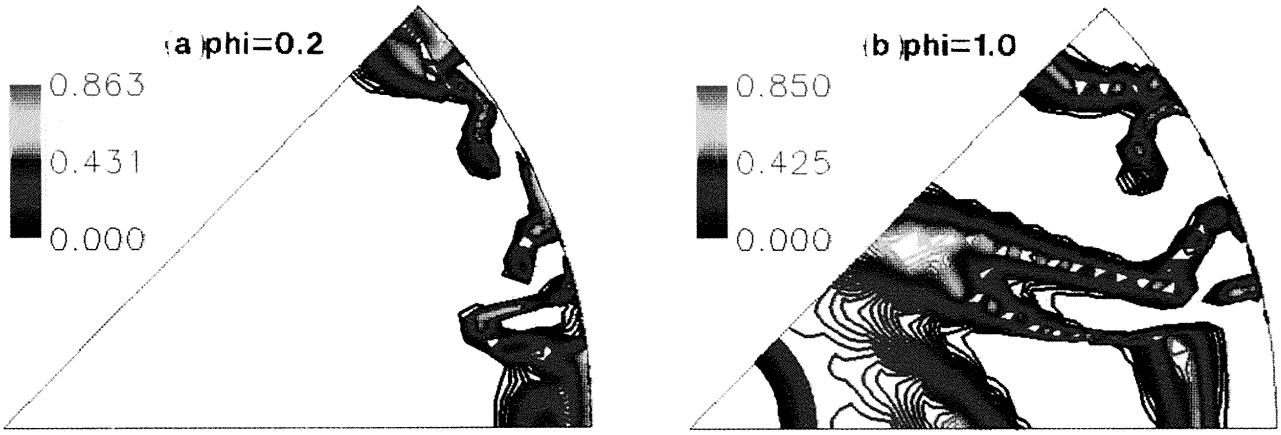

Fig. 21 Contours of OH mass fraction ($\times 100$)(K=65)

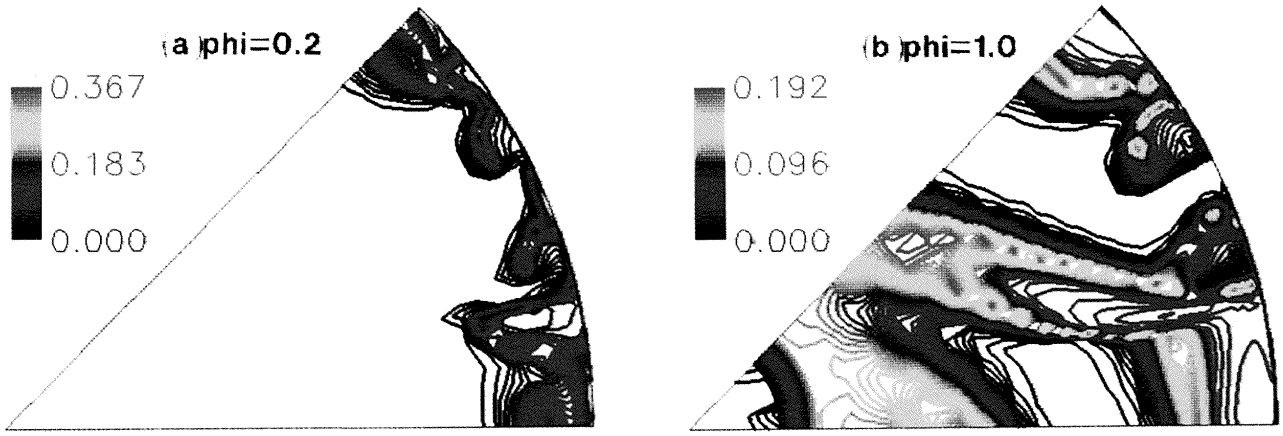

Fig. 22 Contours of NO mass fraction ($\times 100$)(K=65)

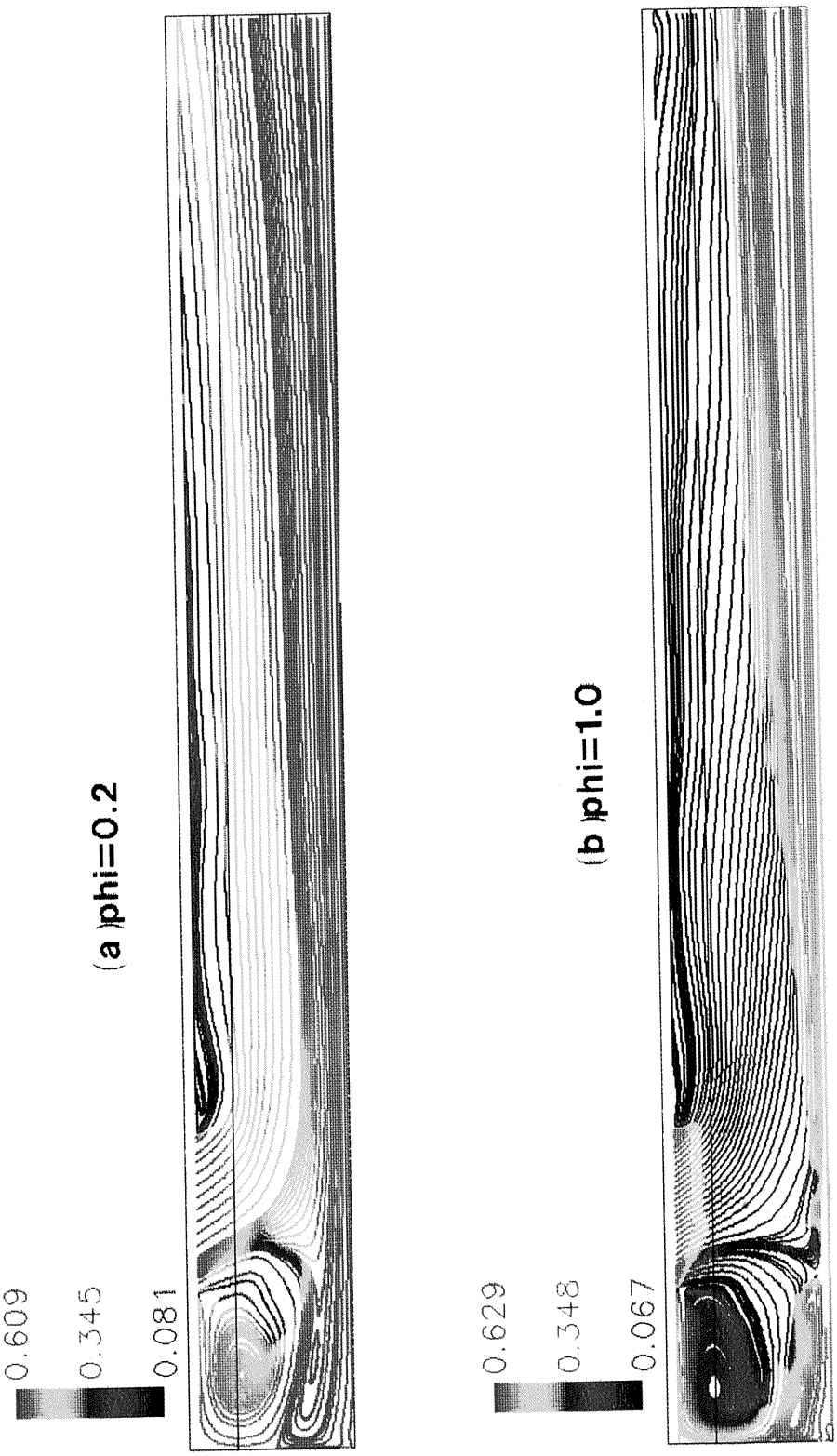

Fig. 23 Streamlines colored by density

the combustor. In both cases the bigger recirculation zone near the end wall is similar while many small recirculation zones are formed in the case of $\phi=1.0$. This could be attributable to combustion generated turbulence. The predicted overall characteristics of the combustor for the two cases studied are summarised in Table II.

11. CONCLUSIONS

(1) A three-dimensional code for the numerical prediction of turbulent reactive flow in jet induced ram combustors is developed.

(2) A Low Reynolds number k-ε model is used for the simulation of turbulence.

(3) Stretched Laminar Flamelet Model based on a detailed reaction mechanism is used to simulate turbulent combustion with finite rate chemistry.

(4) Presumed-PDF method is used to achieve PDF closure of Chemistry

(5) The code is used to compute the steady state characteristics of the combustor.

(6) Simulation results showing the recirculation zones, distribution of species and temperatures are presented for the case of two equivalence ratios.

12. ACKNOWLEDGEMENTS

This work was carried out at the National Aerospace Laboratory under the fellowship of the Science and Technology Agency of Japan. I will like to thank Dr. T. Tamaru, the head of the combustion laboratory, for making me familiar with the experiments on the jet assisted ram combustors and providing useful inputs. Also I will like to acknowledge the help of Mr. T. Yamamoto and Dr. Shunji Enomoto for helping me with the computing facilities of the laboratory. Finally, I will like to express my appreciation for all those who helped me in every way to make my fellowship a very memorable experience.

13. REFERENCES

[1] T. Saito, T. Tamaru, K. Shimodaira, H. Yamada, Y. Kinoshita, Y. Seki & K. Kitahara, "Combustion Characteristics of Jet Induced Type Ram Combustor Using Hydrogen Fuel", Proceedings of Fall Annual Symposium of Gas Turbine Society of Japan (1993).

[2] S. M. Correa & W. Shyy, "Models and Methods for Gaseous Turbulent Combustion", Progress in Energy and Combustion Science 13 (1987), 249-292.

[3] S. Kumar, "A Computer Model in General 3-D Curvilinear for the Prediction of the Turbulent Flow Field in a Jet Induced Ram Combuster", Technical Report TR-1240, National Aerospace Laboratory, Japan, 1994.

[4] T. Yamamoto & T. Tamaru, "Numerical Simulation of Combustion Flow around a Flame Holder with Hydrogen Injection", Technical Report TR-1233, National Aerospace Laboratory, Japan, 1994.

[5] H. K. Myong & N. Kasagi, "A New Approach to the Improvement of k-ε Turbulence Model for Wall-Bounded Shear Flows," International Journal of JSME 33 (1990), 63-72.

[6] C. Chen, J.J. Riley & P.A. McMurthy, "A Study of Favre Averaging in Turbulent Flows with Chemical Reaction", Combustion and Flame 87 (1991), 257-277.

[7] S.B. Pope, "Turbulent Premixed Flames J Annual Review of Fluid Mechanics", 1987.

[8] J.B. Moss, "Simultaneous Measurements of Concentration and Velocity in an Open Turbulent Flame", Combustion Science and Technology 22 (1980), 119-129.

[9] T. Takagi, T. Okamoto, M. Taji and Y. Nakasuki, "Retardation of Mixing and Countergradient Diffusion in a Swirling Flame", Twentieth Symposium (International) on Combustion (1985).

[10] J. Janicka & W. Kollmann, "The Calculation of Mean Radical Concentrations in Turbulent Diffusion Flames", Combustion and Flame 44 (1982), 319-336.

[11] N. Peters, "Laminar Flamelet Concepts in Turbulent Combustion", Twenty-First Symposium (International) on Combustion (1986).

[12] D. Lentini, "Assesment of the Streched Laminar Approach for Non-premixed Turbulent Combustion", AIAA Paper 93-2047, 1993.

[13] R.W. Bilger, "Conditional Moment Closure for Turbulent Reacting Flow", Physics of Fluids 5

(2) (1993), 436-444.

[14] W.E. Mell, V. Nilsen, G. Kosaly & J.J. Riley, "Investigation of Closure Models for Non-premixed Turbulent Reacting Flows", Physics of Fluids 6 (1994), 1331-1356.

[15] C. Montgomery, G. Kosaly & J. J. Riley, "Direct Numerical Simulation of Turbulent Reaction Flow Using a Reduced Hydrogen-Oxygen Mechanism", Combustion and Flame 95 (1993), 247-260.

[16] S.K. Liew, K.N.C. Bray & J.B. Moss, "A Stretched Laminar Flamelet Model of Turbulent Non-premixed Combustion", Combustion and Flame 56 (1984), 199-213.

[17] W.P. Jones & A.Pascau, "Calculation of Velocity, Composition and Temperature Fields in a Model Swirl Combustor with a Reynolds-Stress Transport Turbulence Model", in Heat Transfer in Radiating and Combusting Systems, M.G. Carvalho, F. Lockwood & J. Traine, eds., Proceedings of the EUROTHERM Seminar No.17, Springer Verlag, Oct 1990, 128-145.

[18] D. Lentini, "Validation of a Formulation in Conserved Scalar Space for Stretched Laminar Flamelet Approach", AIAA Paper 93-2200, 1993.

[19] G. Dixon-Lewis & M. Missaghi, "Structure and Extinction Limits of Counterflow Diffusion Flames of Hydrogen-Nitrogen Mixtures in Air", Twenty-Second Symposium (International) on Combustion (1988).

[20] N. Peters, "Laminar Diffusion Flamelet Models in Non-premixed Turbulent Combustion", Progress in Energy and Combustion Science 10 (1984), 319-339.

[21] S. Gordon & B.J. McBride, "Computer Progress for Calculation of Complex Chemical Equilibrium Composition, Rocket Performance, Incident and Reflected Shocks and Chapman-Jouguet Detonation", NASA SP-273, Washington, DC,1971.

[22] J.Y. Chen & W. Kollmann, "PDF Modeling and Analysis of Thermal NO Formation in Turbulent Non-premixed Hydrogen-Air Jet Flames", Combustion and Flames 88 (1982), 397-412.

[23] C.H. Gibson & P.J. Masiello, Lecture Notes in Physics 12 (1972).

[24] S.V. Patankar, in Numerical Heat Transfer and Fluid Flow, Washington, DC, 1980.

TECHNICAL REPORT OF NATIONAL
AEROSPACE LABORATORY
TR-1267T

航空宇宙技術研究所報告1267T号（欧文）

平成7年5月発行

発行所　航空宇宙技術研究所
東京都調布市深大寺東町7－44－1
電話　三鷹(0422)47－5911(大代表)　〒182
印刷所　株式会社　共進
東京都杉並区久我山5－6－17

Published by
NATIONAL AEROSPACE LABORATORY
7-44-1 Jindaiji higashi, Chōfu, Tokyo 182
JAPAN

Printed in Japan